Geophysical Journal International

Geophys. J. Int. (2014) **196,** 1754–1769
Advance Access publication 2013 December 24

doi: 10.1093/gji/ggt478

Variability of dynamic source parameters inferred from kinematic models of past earthquakes

M. Causse,[1] L. A. Dalguer[2] and P. M. Mai[3]

[1] *ISTerre, Université Joseph Fourier, IFSTTAR, F*-38041 *Grenoble, France. E-mail: mathieu.causse@ujf-grenoble.fr*
[2] *Swiss Seismological Service, ETH Zürich, CH*-8092 *Zürich, Switzerland*
[3] *King Abdullah University of Science and Technology, Thuwal* 23955-6900, *Saudi Arabia*

Accepted 2013 November 22. Received 2013 November 20; in original form 2013 January 21

SUMMARY

We analyse the scaling and distribution of average dynamic source properties (fracture energy, static, dynamic and apparent stress drops) using 31 kinematic inversion models from 21 crustal earthquakes. Shear-stress histories are computed by solving the elastodynamic equations while imposing the slip velocity of a kinematic source model as a boundary condition on the fault plane. This is achieved using a 3-D finite difference method in which the rupture kinematics are modelled with the staggered-grid-split-node fault representation method of Dalguer & Day. Dynamic parameters are then estimated from the calculated stress-slip curves and averaged over the fault plane.

Our results indicate that fracture energy, static, dynamic and apparent stress drops tend to increase with magnitude. The epistemic uncertainty due to uncertainties in kinematic inversions remains small ($\phi \sim 0.1$ in $\log_{10}$ units), showing that kinematic source models provide robust information to analyse the distribution of average dynamic source parameters. The proposed scaling relations may be useful to constrain friction law parameters in spontaneous dynamic rupture calculations for earthquake source studies, and physics-based near-source ground-motion prediction for seismic hazard and risk mitigation.

Key words: Earthquake ground motions; Earthquake source observations; Computational seismology.

GJI Seismology

1 INTRODUCTION

The earthquake rupture process distributes accumulated strain energy into fracture energy, radiated seismic energy and heat. In this context, the term 'fracture energy' is a mesoscopic parameter that characterizes energy dissipation phenomena involved in the rupture expansion. Quantifying the energy balance for the dynamic rupture process remains a crucial issue in earthquake seismology, as it strongly affects ground-motion estimation and seismic hazard assessment, because rupture dynamics control the radiated seismic energy.

Current efforts in advanced source modelling aim to adopt basic principles of rupture mechanics, either through so-called 'pseudo-dynamic' models (kinematic models that capture main features of earthquake dynamics, e.g. Guatteri *et al*. 2004; Schmedes *et al*. 2010; Song & Somerville 2010; Mena *et al*. 2012), or by means of fully dynamic spontaneous rupture simulations. The latter approach is computationally demanding, and requires a full description of the initial stress prior to the earthquake as well as the frictional behaviour on the fault that governs the slip weakening process (such as dynamic stress drop, strength excess and slip weakening distance). Both stress and friction on the fault are still poorly known and difficult to constrain with observations.

Several studies have been carried out to characterize the slip weakening behaviour from earthquake source kinematics. The common principle is to retrieve the stress evolution at each point of the fault plane as dictated by the slip history obtained from kinematic inversion (e.g. Bouchon 1997; Ide & Takeo 1997; Day *et al*. 1998; Dalguer *et al*. 2002; Fukuyama *et al*. 2003; Mikumo *et al*. 2003; Ripperger & Mai 2004; Tinti *et al*. 2005a,b). It is important to note that small-scale features of the rupture process cannot be resolved because kinematic inversions are generally performed at low frequency (<1 Hz; Spudich & Guatteri 2004), and require *a priori* choices for certain source parameters, for instance for the shape of the source-velocity function (Piatanesi *et al*. 2004; Tinti *et al*. 2009). Besides, it has been shown that kinematic inversion techniques only provide a gross description of the rupture history (e.g. Mai *et al*. 2007). Certain details of the slip evolution are likely artefacts, introduced by the inherent non-uniqueness of the inverse problem, errors in the forward model parametrization, and modeler-dependent *a priori* choices in the inversion process (e.g. inversion method, smoothing constraints, data selection). Despite these limitations, important efforts have been made to analyse the stress-change fields implied by kinematic models, and to investigate their relationship to the physics of faulting. Kinematic source inversions thus provide a framework for incorporating observational

constraints into earthquake rupture models, and in principle allow for independent estimation of finite-fault stress parameters that can be compared to standard earthquake source studies based on point-source assumptions (e.g. Abercrombie & Rice 2005; Allmann & Shearer 2009). In addition, a major advantage of using extended-source rupture models compared to point source-base studies is that variations in the distribution of energy flux due to directivity effects can be accounted for (Ma & Archuleta 2006). Note also that stress change estimates are physically well defined if computed directly from source-parameter distributions, as then they are not affected by spectral-domain measurement errors on corner frequency. In point-source estimation of stress drop, using corner frequency and a specific spectral decay model, small uncertainties in corner frequency map into large uncertainties in stress drop (e.g. Prieto *et al*. 2007).

The goal of this study is not to investigate the space–time details of the dynamic earthquake rupture process. Instead, we aim to constrain average, global dynamic source properties, and to examine their distribution and potential scaling properties. We assess fracture energy, static and dynamic stress drops, as well as apparent stress drop from a set of past earthquakes for which finite-source rupture models are available. We carry out several tests to determine if kinematic inversion models of limited resolution may still carry useful information on the scaling of dynamic source properties. We take advantage of a large earthquake rupture model database (now at http://equake-rc.info/srcmod/), and analyse a suite of 31 rupture models from 21 crustal events with various styles of faulting, and with M_w ranging from 5.7 to 7.7. We propose empirical models defining the distribution of fracture energy, static and dynamic stress drops that may be useful in advanced source modelling for ground-motion simulation (such as 'pseudo-dynamic' models or spontaneous rupture simulations). Finally, we investigate if the inferred dynamic properties exhibit any relation with respect to geologically observable quantities, like cumulative slip on fault.

2 METHOD

2.1 Principle

Our strategy is to constrain average dynamic properties from a set of earthquakes for which finite-source rupture models are available. The principle is first to retrieve the spatio-temporal shear stress distribution from source kinematics to constrain the spatial distribution of dynamic parameters on the fault plane. Those parameters are then averaged over the slipping area, and analysed with respect to seismic moment.

Shear-stress histories are locally computed via the elastodynamic equations of motion using the slip velocity distribution from kinematic inversion as a boundary condition on the fault plane (Fig. 1). This is achieved by applying a 3-D finite difference method that uses the traction-at-split-node method adapted to the velocity-stress staggered-grid finite difference scheme (Dalguer & Day 2007). The code, initially developed for spontaneous dynamic rupture simulations, has been modified to be suitable for such kinematically constrained calculations, referred to as '3-D forward kinematic' calculations in the following. Note that perfectly matched layers absorbing boundaries are implemented in the code to avoid reflected waves at the boundaries of the modelled volume.

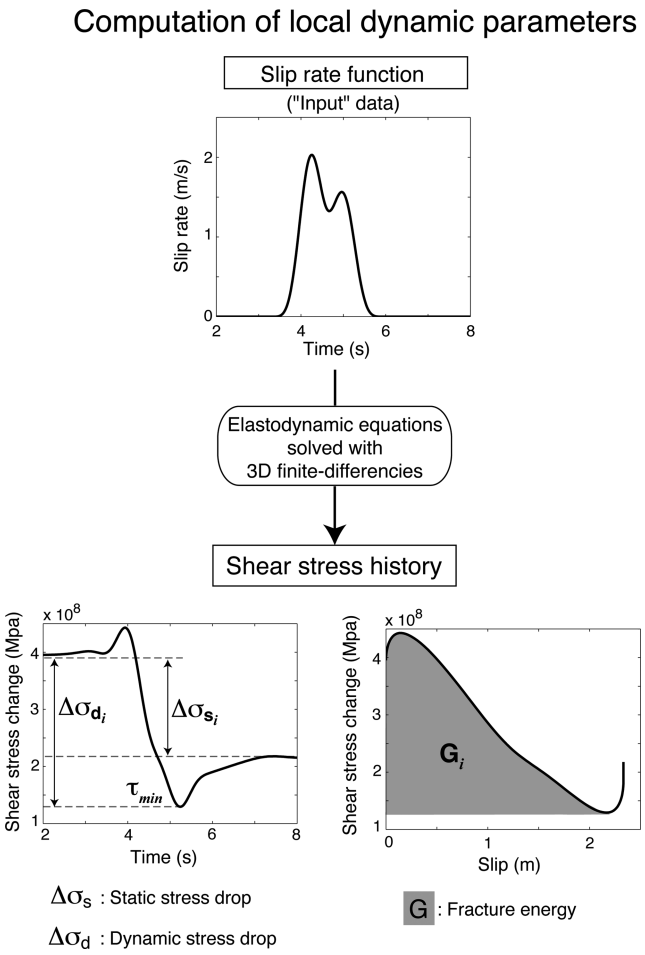

Figure 1. Conceptual workflow for computing fracture energy and stress drop at a given point i on the fault plane, based on the slip rate function obtained from kinematic source inversion. Fracture energy then corresponds to the shaded area (bottom right).

2.2 Dynamic source parameters

The following parameters are computed: static stress drop $\Delta\sigma_s$ (difference between initial and final shear stress), dynamic stress drop $\Delta\sigma_d$ (difference between initial and minimal shear stress occured during the slip evolution) and fracture energy G (Fig. 1). Those parameters are first locally computed, and then averaged over the fault plane. In the following, the average of the computed dynamic properties will be denoted by $\bar{G}$, $\overline{\Delta\sigma_s}$, $\overline{\Delta\sigma_d}$, $\overline{\Delta\sigma_A}$.

Our definition of fracture energy is equivalent to the breakdown work defined by Tinti *et al*. (2005a):

$$G = \int_0^T (\tau(t) - \tau_{\min}) \cdot \dot{u}(t) \mathrm{d}t, \quad (1)$$

where $\tau(t)$ is the shear stress history, $\dot{u}(t)$ is the slip velocity and T_b is the time corresponding to the minimum traction $\tau_{\min}$ achieved during during the slipping phase. G represents the 'seismological fracture energy'. As such, it characterizes several processes occurring at the expanding crack tip such as micro-cracking, off-fault plasticity, energy loss due to heat and other energy dissipative phenomena (Cocco *et al*. 2006; Cocco & Tinti 2008). It thus represents a mesoscopic parameter that contains all dissipative processes in the volume surrounding the crack tip, but mapped onto the fault plane. Therefore, due the scale of the fault and its complexity, it

needs to be understood as a 'phenomenological' parameter. However, this partitioning of 'seismological fracture energy' does not affect the global earthquake energy balance, defined in terms of energy density as $E_S = (\Delta\sigma_d - \Delta\sigma_s/2) \cdot D - G$, where E_S is the radiated seismic energy per unit of fault area and D, $\Delta\sigma_d$, $\Delta\sigma_s$, G are the final slip, dynamic and static stress drops and fracture energy over the fault plane, respectively. Including the definition of apparent stress drop, $\Delta\sigma_A = \mu \frac{E_S \cdot A}{M_0}$, where A is the fault area, we obtain a relation between apparent stress-drop and fracture energy:

$$\Delta\sigma_A = (\Delta\sigma_d - \Delta\sigma_s/2) - \frac{G}{D}. \quad (2)$$

2.3 Data and data preparation

To analyse the distribution and scaling of the average dynamic parameters, we use a dataset of 31 finite-source rupture models obtained by kinematic inversion, from 21 crustal events with various styles of faulting (Table 1). Rupture models have been selected based on the availability of a complete rupture history in space and time. Source models derived from inversion of teleseismic data, whose spatio-temporal resolution is in general limited, have been dismissed (except the model of Dreger (1994) for the 1994 Northridge earthquake, which is included to complete the analysis of the epistemic uncertainty due to variations in the input kinematic models). Also, rupture models obtained on segmented/curved faults have been 'flattened' and mapped onto a single planar fault surface.

Since such rupture models are usually obtained on coarse grids (∼1–10 km), they need to be interpolated to ensure stability in the 3-D numercial calculations to accurately retrieve the shear-stress history. We chose various grid interpolations, ranging from 50 m (for small events, having short rise time and thus needing a good spatial resolution) to 300 m (for the largest events). Because the inferred dynamic parameter values may be affected by the particular pre-processing choices for the source models, we test different interpolation schemes: linear, cubic, zero-padding and 'k-square'. The later assumes self-similarity of the static slip beyond the Nyquist wavenumber of the original model by imposing a k^{-2} slope of the slip spectrum. The impact of the static slip interpolation is first investigated on the model of Semmane *et al*. 2005b (referred to as Sem05b in the following) for the 2000 Tottori earthquake. From the different models, we then compute $\bar{G}$, $\overline{\Delta\sigma_s}$ and $\overline{\Delta\sigma_d}$ whose values in principle may be affected by the corresponding interpolation procedures.

Our tests reveal that average dynamic parameters are almost insensitive to the adopted slip interpolation method (Fig. 2 and Table 2). The interpolation tends to decrease average slip in fault regions in which the 2nd spatial derivative of slip is large. Consequently, as proposed by Tinti *et al*. (2005a), we adopt an iterative procedure to scale the original slip distribution until the interpolated slip averaged on a given subfault reaches the initial slip value. We

Table 1. Source inversion models used in this study. Events and source models were selected from the database of finite-source rupture models (http:/equake-rc.info/srcmod), except for Miyagi-Iwate Nairiku.

Event	Location	Date	M_w	Reference
1	Iwate-Miyagi Nairiku	2008 June 14	6.9	Suzuki *et al*. (2010)
2	Fukuoka	2005 March 20	6.7	Asano & Iwata (2006)
3	Parkfield	2004 September 28	6.0	Custodio *et al*. (2005)
4	Boumerdes	2003 May 21	7.2	Semmane *et al*. (2005a)
5	Tottori	2000 October 06	6.7	Semmane *et al*. (2005b)
6	Tottori	—	—	Iwata & Sekiguchi (2002)
7	Izmit	1999 August 17	7.6	Delouis *et al*. (2002)
8	Izmit	—	—	Bouchon *et al*. (2002)
9	ChiChi	1999 September 20	7.6	Zhang *et al*. (2004)
10	ChiChi	—	—	Ma *et al*. (2001)
11	ChiChi	—	—	Chi *et al*. (2001)
12	Yamaguchi	1997 June 25	5.8	Miyakoshi *et al*. (2000)
13	Kagoshima	1997 March 26	6.0	Miyakoshi *et al*. (2000)
14	Kagoshimaen-hobu-seibu	1997 May 13	6.1	Horikawa (2001)
15	Colfiorito 1	1997 September 26	5.7	Hernandez *et al*. (2004)
16	Colfiorito 2	1997 September 26	6.0	Hernandez *et al*. (2004)
17	Colfiorito 3	1997 October 14	5.9	Hernandez *et al*. (2004)
18	Kobe	1995 January 17	6.9	Wald (1996)
19	Kobe	—	—	Yoshida *et al*. (1996)
20	Northridge	1994 January 17	6.8	Wald *et al*. (1996)
21	Northridge	—	—	Hartzell *et al*. (1996)
22	Northridge	—	—	Dreger (1994)
23	Landers	1992 June 18	7.2	Wald & Heaton (1994)
24	Landers	—	—	Hernandez *et al*. (1999)
25	Landers	—	—	Cotton & Campillo (1995)
26	Loma Prieta	1989 October 18	6.9	Wald *et al*. (1991)
27	Saguenay	1988 November 25	5.8	Hartzell *et al*. (1994)
28	North Palm Springs	1986 July 08	6.1	Hartzell (1989)
29	Imperial Valley	1979 October 15	6.5	Hartzell & Heaton (1983)
30	Imperial Valley	—	—	Archuleta (1984)
31	Coyote Lake	1979 August 06	5.9	Liu & Helmberger (1983)

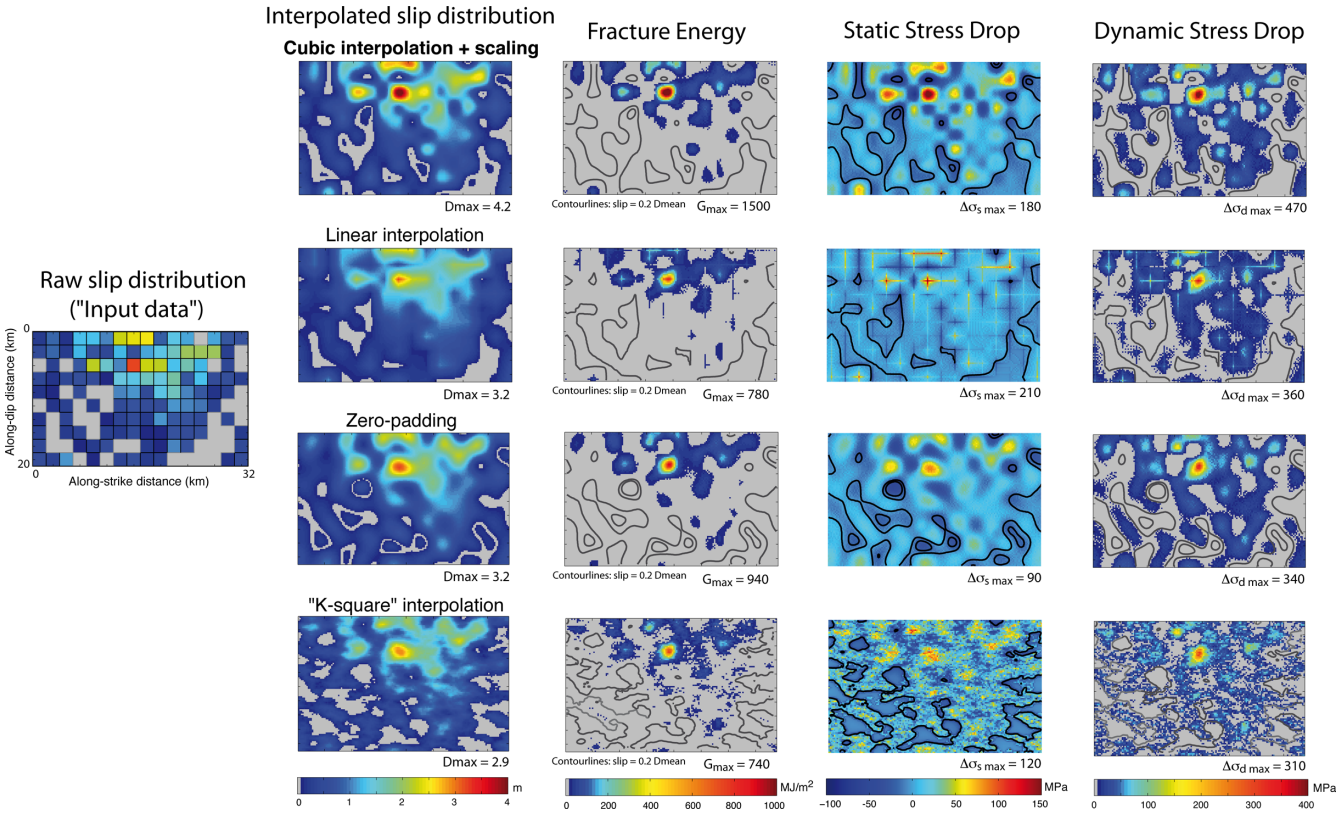

Figure 2. Effect of the chosen final-slip interpolation scheme on inferred dynamic parameter distributions. The figures correspond to Sem05b's source inversion model for the 2000 Tottori earthquake. Dynamic parameters are averaged on a surface with slip above 20 per cent of the mean slip, defined by the contour lines (roughly corresponding to the surface of non-zero slip of the original slip model). The average values are summarized in Table 2. « k-square » is obtained by assuming a k^{-2} slope of the static slip spectrum beyond the Nyquist frequency of the original model. « Cubic + scaling » refers to an iterative procedure used to preserve seismic moment on each subfault (top row).

Table 2. Sensitivity of the average dynamic parameters values (fracture energy, static and dynamic stress drops) to the adopted static slip interpolation procedure. The values are for Sem05b's source model for the 2000 Tottori earthquake (see Fig. 2). The procedure adopted in the following is 'cubic + scaling' that preserves seismic moment on each subfault.

Slip interpolation scheme	G (MJ m^{-2})	$\Delta\sigma_s$ (MPa)	$\Delta\sigma_d$ (MPa)
Linear	14	5	16
Zero-padding	17	5.5	18
k-square	16.5	8.5	22
Cubic	16.5	6	17
Cubic + scaling	22	7.5	21

remark that this approach yields slightly higher dynamic parameter values (∼20 per cent).

The interpolation procedure requires two steps for source models derived with spatially variable rake angles. The most natural way to proceed, adopted here, is to first calculate slip along-strike and along-dip, and then to interpolate both slip distributions. Another possibility is to interpolate final slip and rake, and then calculate slip along-strike and along-dip. We estimate dynamic parameters for the Wald (1996) model for the 1995 Kobe earthquake using these two approaches. Choosing procedure 1 or 2 does not strongly affect the results (procedure 2 results in 15–20 per cent reduction of fracture energy and dynamic stress drop).

After performing the spatial slip interpolation, the slip rate functions (SRFs) are defined on each point on the fault from the functional form employed in the specific inversion study. Stability conditions of the finite-difference calculations implies very short time steps (between 0.005 and 0.015 s for the larger events). Therefore, smoothing of the SRFs is needed to avoid introducing high frequencies that are not resolved in the inverted source models. This is achieved by convolution with a hamming window of length $T_{\mathrm{hamm}} = 1/F_{\max}$, where $F_{\max}$ is the maximum frequency used in the inverted data.

Once the input kinematic models have been interpolated, the dynamic parameter distributions are obtained from the shear-stress time histories of the forward kinematic rupture calculations. Since kinematic models povide information about the stress changes only, and not about the absolute stress values, we need to make some assumption to define the initial stress. As proposed by Tinti *et al.* (2005a), the initial stress is supposed to be colinear with the slip direction. As for input kinematic models with temporally and/or spatially variable rake angles, we chose an initial stress colinear with the final slip, and with a large value (500 MPa) to minimize the angle between the total traction and the slip velocity.

Finally, average dynamic parameters are extracted by calculating their mean value $\bar{G}$, $\overline{\Delta\sigma_s \Delta\sigma_d}$ and $\overline{\Delta\sigma_A}$ over the slipping area. We define the slipping area as the zone that slipped more than 20 per cent of the mean slip value. This particular choice is motivated by the fact that this area approximately corresponds to the surface region of the original slip distribution with non-zero slip. Mai *et al.* (2006) use area with slip above 33 or 66 per cent of the maximum slip, because these regions are supposedly better resolved in source inversion. However, maximum slip is generally less well resolved than average slip, which thus may introduce an additional bias.

3 SENSITIVITY ANALYSIS

The purpose of this section is to show the sensitivity of inferred dynamic parameters due to uncertainties and variations in the input kinematic models.

3.1 Sensitivity to the roughness degree of slip heterogeneity

To quantify the sensitivity of average dynamic parameters to slip roughness we generate synthetic 'k-squared' kinematic models (e.g. Causse *et al*. 2009) with various degrees of slip roughness, and compute their dynamic properties using the procedure described in Section 1 (Fig. 3). The slip roughness is expressed in term of the corner wavenumber (k_c) of the slip amplitude spectrum, controlled by the non-dimensional parameter K: $k_c = K/\sqrt{(L^2 + W^2)}$. The inverse of k_c represents a characteristic scale of the slip distribution. For increasing K, the resulting slip maps become rougher, and are characterized by enhanced small-scale complexity. The phase angles of the slip spectrum are randomly chosen, but are similar for each slip distribution. The source-velocity function is assumed triangular with a constant rise time of 1 s. The rupture velocity is sub-shear, set to 3 km s^{-1}.

Our tests reveal that maximum values of static and dynamic stress drops increase with increasing k_c (or K). Because stress drop is proportional to the derivative of static slip, and larger values of k_c result in stronger fluctuations of static slip at small scales, stress changes will increase with increasing k_c. This is corroborated by Burjanek & Zahradnik (2007) from analysing the dynamic stress fields implied by k-squared source models and by Noda *et al*. (2013), who investigated the sensitivity of the average stress drop measures to the level of slip heterogeneity. A less intuitive result is that $\bar{G}$ also increases with slip roughness. This is consistent with the study of Rice *et al*. (2005) that shows for pulse like source models: $G_i \propto D_i^2$, where G_i and D_i denote local fracture energy and slip, respectively. One then expects $\bar{G}$ to be sensitive to the spatial distribution of static slip. The theoretical relationship of Rice *et al*. (2005) has been recently verified by Bizzarri (2010) for a large number of constitutive models, using 3-D spontaneous dynamic rupture simulations. Additionally, pronounced spatial correlation between G and D^2 has been inferred from numerical simulations (Tinti *et al*. 2005a, see their fig. 11). Using the distributions of dynamic source parameters shown in Fig. 3, we estimate the average apparent stress drop from eq. (2). It scales with slip roughness, with values of $\overline{\Delta\sigma_A}$ of 0.9, 1.7 and 3.2 MPa for $K = 0.5$, 0.8 and 1.3 respectively. This particular scaling of apparent stress suggests that rough (i.e. more heterogeneous) slip distributions more effectively radiate high-frequency seismic energy.

3.2 Rupture velocity

In the approach adopted in our study, rupture velocity is not an outcome of the 3-D forward kinematic calculations, but is imposed as a boundary conditions. Slow rupture expansion generates high stress peak (or yield stress) at the rupture front, and accordingly tends to increase the fracture energy; slow rupture also results in lower minimum stress (or breakdown stress), and consequently gives rise to higher dynamic stress drop. We therefore conduct sensitivity tests assuming various rupture velocities to quantify the effects of potential uncertainties in the inverted rupture times. The results are summarized in Table 3. As a conclusion, $\bar{G}$ and $\overline{\Delta\sigma_d}$ are not strongly affected by small variations of average rupture velocity or small-scale perturbations of the rupture front. Changes of ±10 per cent in rupture speed yield only 3–5 per cent variation in the dynamic parameters.

3.3 SRF and rise time

The shape of the inferred stress histories is influenced by the shape (functional form and rise time) of the SRF (e.g. Tinti *et al*. 2005b). A sharp initial rise of the SRF results in high yield stress, and a sharp decrease generates large dynamic stress drop, that is strong overshoot effects. Thus, short rise times generate large peak slip-rate, and thus larger $\bar{G}$ and $\overline{\Delta\sigma_d}$. Our calculations may thus be affected by the *a priori* choice of the SRF in kinematic inversions, as well as by potential uncertainties in the rise time. We therefore compute $\bar{G}$ and $\overline{\Delta\sigma_d}$ assuming various slip-rate functions, for the 2000 Tottori earthquake (Sem05b model). Table 4 displays the values of $\bar{G}$ and $\overline{\Delta\sigma_d}$, and Fig. 4 presents the SRFs in the time and frequency domain as well as the inferred shear stress histories and friction laws at the maximum slip zone. Fig. 4 (top) indicates that the shape of the SRF cannot be resolved by Sem05b inversion, matching strong-motion data only up to 0.4 Hz. As shown in Table 4, the values of $\bar{G}$ and $\overline{\Delta\sigma_d}$ are stable if a causal SRF is used, but the use of a non-causal 'smooth ramp' leads to much smaller values. However, these discrepancies are diminished by low-pass filtering (smoothing) of the SRFs. Although this procedure somewhat underestimates the values of $\bar{G}$ and $\overline{\Delta\sigma_d}$, a 'smoothened' data set is more suitable for mutually comparing source models and analysing the scaling of dynamic source properties.

4 SCALING OF SOURCE PARAMETERS

4.1 Scaling of average fracture energy

To investigate the scaling of fracture energy, we derive a simple empirical model of the form: $\log_{10}(\bar{G}) = a\,\log 10(M_0) + b$, by applying a least-square regression (Fig. 5). In our data set, composed of 31 source models from 21 earthquakes, seven events have more than one published source model. Performing regression using each of the 31 models separately would then require attributing weights to the individual earthquakes. Therefore, we compute specific empirical models for the seven multiple-model events, and then derive a single average estimation for the corresponding (M_0, $\bar{G}$) couple. Our analysis returns that $\bar{G}$ increases with seismic moment, such as:

$$\log_{10}(\bar{G}) = 0.60\log_{10}(M_0) - 11.6. \quad (3)$$

This relationship is similar to the one derived by Cocco & Tinti (2008), using a suite of 18 finite-source rupture models from 13 events. We obtain slightly higher values for the coefficients a and b, most likely because Cocco & Tinti (2008) average fracture energy over the entire fault plane, and not only over the slipping area. We also investigate the scaling of $\bar{G}$ with average slip D_m (Fig. 5), and find:

$$\log_{10}(\bar{G}) = 1.35\log_{10}(D_m) + 1.15, \quad (4)$$

valid for D_m in the range $0.05 \leq D_m \leq 4.0$ m. For large events ($D_m > 1$ m), this model is very close to the one derived by Mai *et al*. (2006), $\log_{10}(\bar{G}) = 0.87\ \log_{10}(D_m) + 0.28$, obtained from a set of spontaneous dynamic rupture calculations that closely match target kinematic inversion models (12 models from 9 events). We

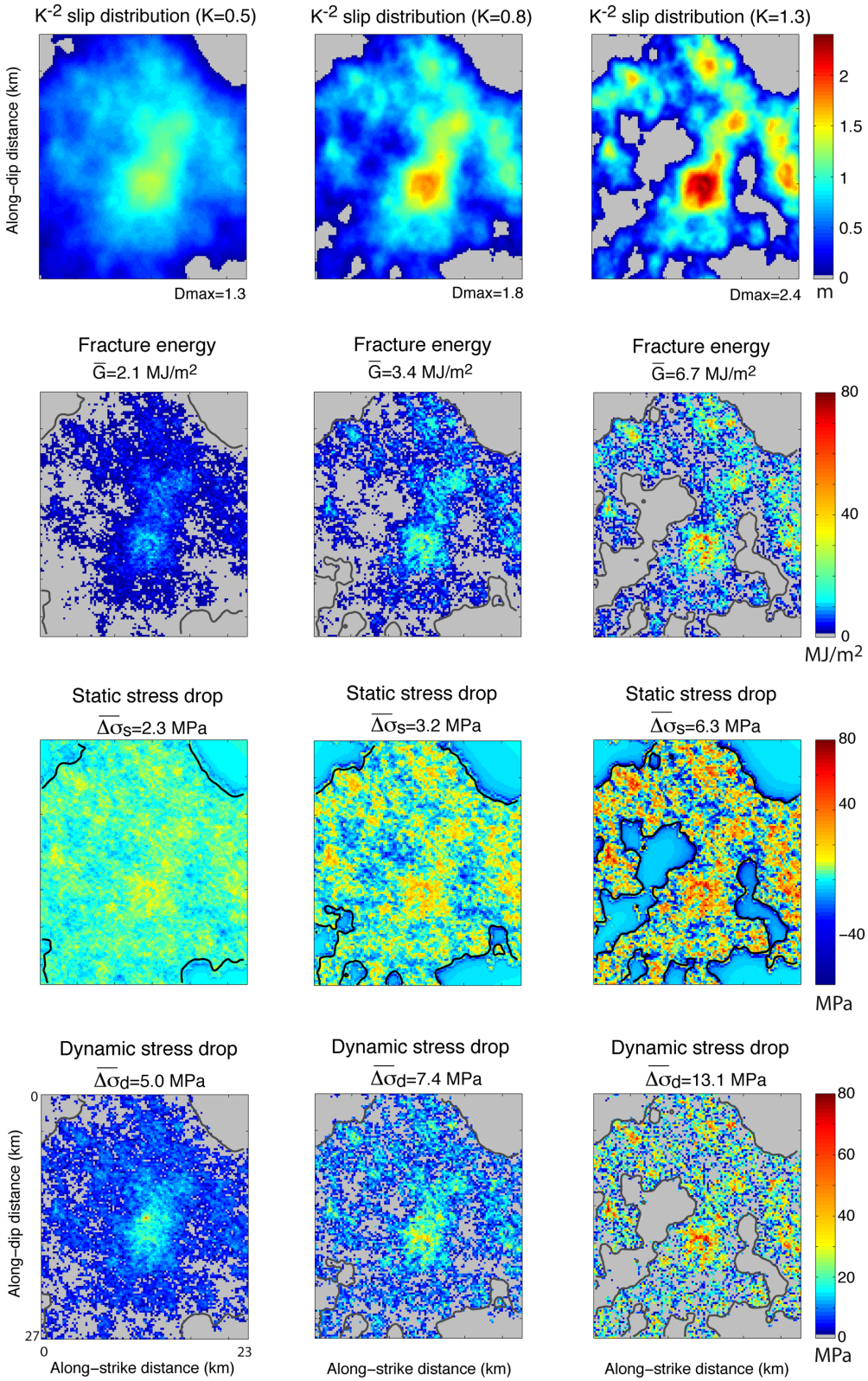

Figure 3. Effect of the roughness degree of static slip heterogeneities on the inferred dynamic parameters. The three synthetic kinematic models (top) are based on k^{-2} static slip distributions (with identical phase spectra). The mean slip equals 0.5 m. Rise time and rupture velocity are constant (1 s and 3 km s^{-1}, respectively). The rupture velocity is sub-shear. The roughness degree of slip is constrained by the position of the corner wavenumber of the slip spectrum: $k_c = K/\sqrt{(L^2 + W^2)}$. The bottom figures show the computed dynamic parameter distributions, as well as their average values, calculated on the area with slip above 20 per cent of the mean slip (this surface is defined by the contour-lines). The average values of apparent stress $\Delta\sigma_A$ are 0.9, 1.7 and 3.2 MPa for $K = 0.5$, 0.8 and 1.3, respectively.

Table 3. Sensitivity of average dynamic parameters (fracture energy and dynamic stress drops) to the rupture time distribution for different kinematic source models. Uncertainties on the rupture time distributions expected in kinematic inversions are represented by ±10 per cent variations on the average rupture velocity (for the model by Wald & Heaton 1994), or by including ±10 per cent randomness in the original rupture times (for Sem05b model).

Source model	Rupture time distribution	G (MJ m^{-2})	$\Delta\sigma_d$ (MPa)
Landers 1992 (Wald & Heaton 1994)	$V_r = 2400$ m s^{-1}	97	34
	$V_r = 2700$ m s^{-1}	94	33
	$V_r = 3000$ m s^{-1}	90	32
Tottori 2000 (Sem05b)	Original model	22	21
	±10 per cent perturbations	25	23

Table 4. Values of average dynamic parameters obtained for the 2000 Tottori event (Semmane *et al*. 2005b) using different slip-rate functions. T_{acc} indicates the duration of the acceleration phase, expressed as a fraction of the total rise time. The SRF low-pass filtering is achieved by convolution with a 1 s Hamming window, representing low-pass filtering of the SRFs below 1 Hz, the maximum frequency inverted in Sem05b.

Type of slip-rate function (SRF)	G (MJ m^{-2})	$\Delta\sigma_d$ (MJ)
SRF not filtered		
Smooth ramp (used by Semmane *et al*. 2005b)	22.5	21
Boxcar	43	35
Triangle	41	33
Regularized Yoffee (Tinti *et al*. 2005b, $T_{acc} = 0.2T_{rise}$)	42	35
Asymmetric cosine ($T_{acc} = 0.2T_{rise}$)	36	30
Asymmetric cosine ($T_{acc} = 0.5T_{rise}$)	43	34
SRF low-pass filtered at 1 Hz		
Asymmetric cosine ($T_{acc} = 0.5T_{rise}$)	27	24
Smooth ramp	21	20

also compare our model to the study of Abercrombie & Rice (2005) that uses point-source models. They report $\log_{10}(G') = 1.28\log_{10}(D_m) + 0.72$, where the quantity G' is derived from the energy balance between fracture energy, static and apparent stress drops, assuming a simple linear slip-weakening friction law. In their work, static stress drop and radiated energy are measured from 30 earthquakes recorded at a borehole station (2.5-km depth) at less than 15 km. Although their inferred G' values are smaller than our $\bar{G}$ estimates (factor ∼2), the overall scaling (i.e. the slope a) is very similar, indicating a clear increase with magnitude. The shift (difference in intercept b) may arise because Abercrombie & Rice (2005) assume a simple linear slip-weakening model for a point source, and thereby neglect the transient dynamic stress variation in space and time of the finite fault ruptures. Their quantity G' may thus underestimate the total fracture energy. Note also that their work is based on smaller magnitude earthquakes ($M_w \sim 0$–7).

4.2 Scaling of static and dynamic stress drops

Numerous studies, considering mostly point-source models, corroborate that the common hypothesis of 'self-similarity' (i.e. scale independence of stress drop) applies for earthquakes of all sizes (e.g. Brune 1970; Somerville *et al*. 1999; Kanamori & Brodsky 2004; Allmann & Shearer 2009). In this case, static and dynamic stress drops would be independent of seismic moment. In contrast, recent analysis of slip distributions measured at the surface after earthquakes or derived from source inversion models indicate that stress drop, related to strain-drop or *D-L* measurements, are highly variable (e.g. Manighetti *et al*. 2007), and thus the hypothesis of self-similarity may not hold for all types of events. Kanamori & Riviera (2004) demonstrated that constant stress drop scaling is inappropriate for a wide magnitude range. An independent study of Dalguer *et al*. (2008), who calibrated dynamic rupture models to match statistical properties of past earthquakes derived from kinematic source inversion models, shows that average stress drop is independent of earthquake size for buried earthquakes, but scale dependent for surface-rupturing earthquakes. This work suggests that buried earthquakes may follow self-similarity scaling, while surface-rupturing earthquakes break self-similarity. Recently, Candela *et al*. (2012a) related stress drop to the scaling properties of fault-surface topography. Using high-resolution laser distance meter measurements on two exhumed faults, they found that fault-surface topography is scale dependent (fault 'roughness' is larger at small scale). Consequently, they propose that stress drop should decrease with increasing source dimension. In contrast, Drouet *et al*. (2011) analysed a seismic sequence following an M_w 6.3 event in the French West Indies, claiming that Brune's stress drop increases with moment magnitude, with the rate of increase diminishing for high magnitudes. This is also suggested by the studies of Mayeda & Malagnini (2009, 2010), using the coda source ratio method.

Using least-square regression from our data set, we obtain the following empirical relationships for the scaling of static and dynamic stress drops (Fig. 6):

$$\log_{10}\left(\overline{\Delta\sigma_S}\right) = 0.18\ \log_{10}(M_0) - 2.7, \tag{5}$$

$$\log_{10}\left(\overline{\Delta\sigma_d}\right) = 0.24\log_{10}(M_0) - 3.5. \tag{6}$$

These indicate that stress drop tends to increase slightly with seismic moment. This tendency is consistent with the studies of

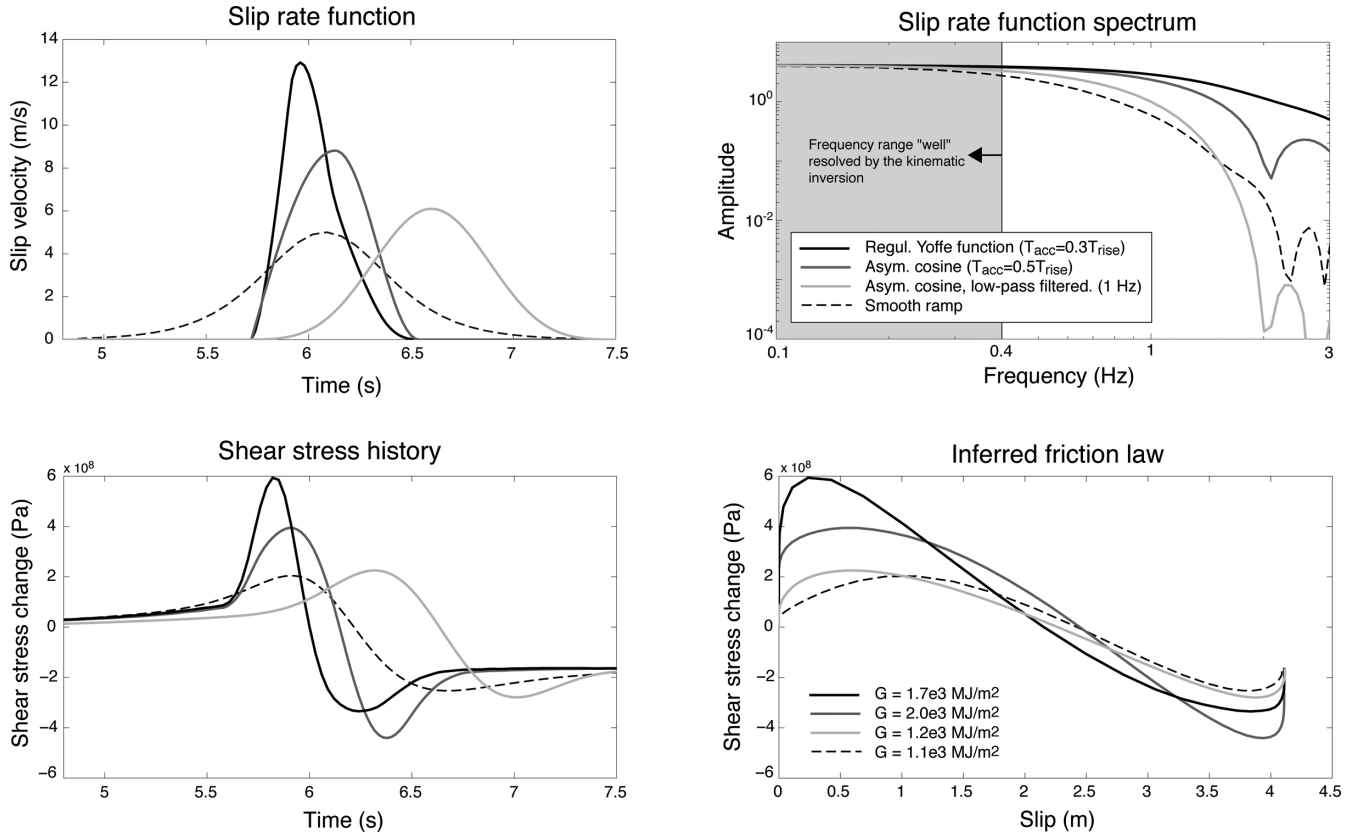

Figure 4. Inferred shear stress history and friction law at the maximum slip zone for the 2000 Tottori earthquake (Semmane *et al*. 2005b), using different *a priori* slip-rate functions. T_{acc} refers to the duration of the slip acceleration phase, expressed as a fraction of the total rise time T_{rise}. Semmane *et al*. 2005b use a smooth ramp (dashed line). Slip-rate functions are also shown in the frequency domain (top right). The gray area represents the frequency range resolved by the kinematic inversion (0.1–0.4 Hz, see Fig. 9 of Semmane *et al*. 2005b for more details).

Mai *et al*. (2006) and Abercrombie & Rice (2005). Note however that stress drop values scatter significantly (the coefficients of determination for the static and apparent stress drops are $R^2 = 0.17$ and $R^2 = 0.24$, respectively, indicating that the regression line does not fit the data very well). The average dynamic stress drop is larger than average static stress drop due to undershoot effects (e.g. Kanamori & Riviera 2006). By least square regression, we obtain: $\overline{\Delta\sigma_d} = 1.5\Delta\sigma_S + 3$ (with stress drops expressed in MPa). However, the exact relationship depends on the fault plane area on which stress drop is averaged. The difference between dynamic and static stress drops becomes smaller when using only the fault regions with positive static stress drop.

4.3 Scaling of apparent stress drop

The apparent stress drop represents the density of radiated seismic energy per unit of slip. It is of fundamental interest for seismic hazard, since it directly pertains to the level of ground motion at intermediate frequencies. We then compute $\overline{\Delta\sigma_A}$ according to eq. (2). As pointed out by Ide (2002), using kinematic rupture models inherently leads to substantial underestimation of the actual radiated seismic energy, because certain small-scale details of the rupture process—like abrupt variations of the rupture velocity generating high frequency—can not be resolved. For the 1995 Kobe earthquake, the values of Ide (2002) are threefold smaller than the ones derived from other studies based on integration of far-field waveforms. In our study, input kinematic source models are initially 'smoothened' (see Section 2.3). The values of $\overline{\Delta\sigma_A}$ are hence likely biased downward. Indeed, we obtain negative apparent stress-drop for some models. We then average $\Delta\sigma_A$ over the fault area with positive static stress drop (area of potential radiation of seismic energy). Still, six source models remain with negative values for $\overline{\Delta\sigma_A}$; those models are excluded from the subsequent analysis. As an illustration of the effect of the input data 'smoothing,, the models of Sem05b for the Tottori earthquake returns $\overline{\Delta\sigma_A} = 1.5$ MPa, which becomes $\overline{\Delta\sigma_A} = 2.7$ MPa if a cosine SRF (low-pass filtered) is assumed, and $\overline{\Delta\sigma_A} = 4.2$ MPa if a cosine SRF (not filtered) is assumed.

The scaling of $\overline{\Delta\sigma_A}$ is represented on Fig. 7, as well as the scaling of the quantity $\overline{\Delta\sigma_d} - \overline{\Delta\sigma_d}/2$ (i.e. available elastic energy per unit of slip). The ratio $\left(\overline{\Delta\sigma_d} - \overline{\Delta\sigma_d}/2\right)/\overline{\Delta\sigma_A}$ (related to the inverse of radiation efficiency) is around 10–15, which means that the radiation efficiency is less than 0.1, that is, less than 10 per cent of the available elastic energy is radiated as seismic energy. In the case of $\Delta\sigma_d = \Delta\sigma_S$ (no undershoot or overshoot effects), Abercrombie & Rice (2005) obtain $1/2 \cdot \overline{\Delta\sigma_s}/\overline{\Delta\sigma_A} \approx 5$, which corresponds to 20 per cent of radiated seismic energy. This discrepancy is likely due to the low-pass filtering of our input data.

Regardless of the underestimation of the inferred $\Delta\sigma_A$ values, the least-square regression of our data set suggests a scale dependence of the apparent stress drop, which slightly increases with seismic moment (the coefficient of determination is $R^2 = 0.50$). This tendency is also suggested by Abercrombie & Rice (2005) for $M_w \sim 0$–7, and corroborated by Drouet *et al*. (2011), who also found that the rate of increase diminishes for $M_w > 4.5$–5.

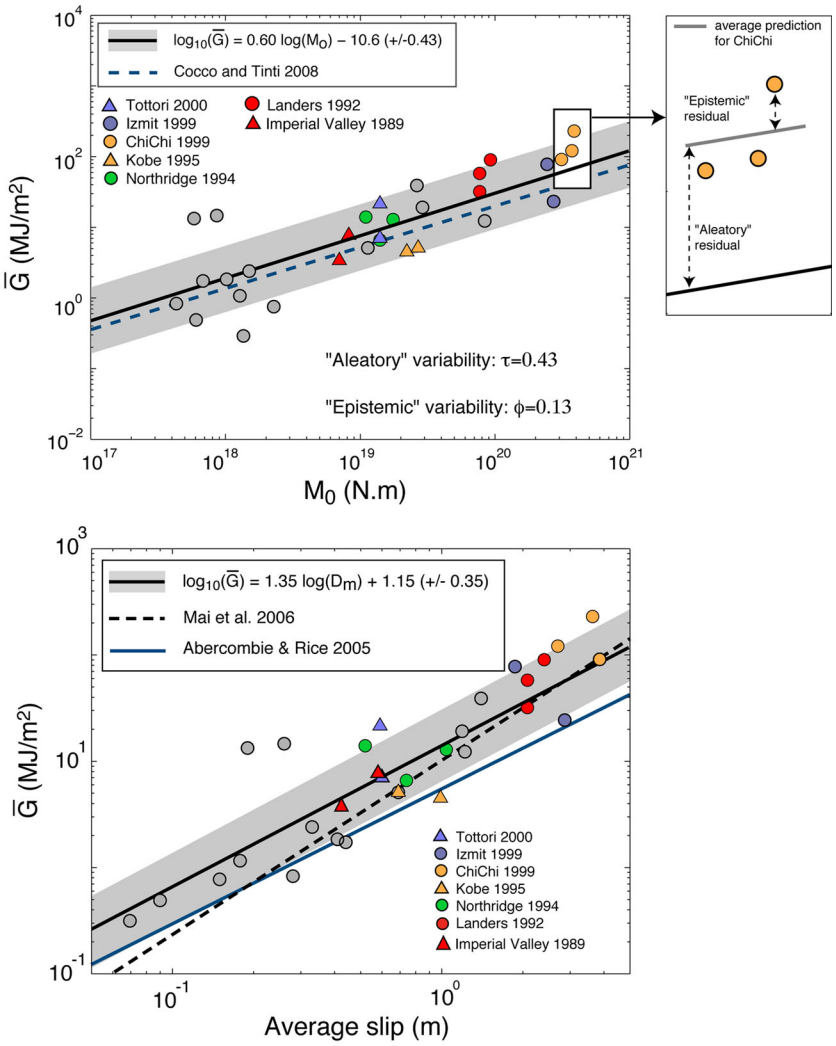

Figure 5. Empirical model proposed for the average fracture energy G with respect to seismic moment (top) and mean slip (bottom). The models are compared with previous studies of Cocco & Tinti (2008) (blue dashed line), Abercrombie & Rice (2005) (blue solid line) and Mai *et al*. (2006) (black dashed line). The gray circles indicate events for which only a single model is available.

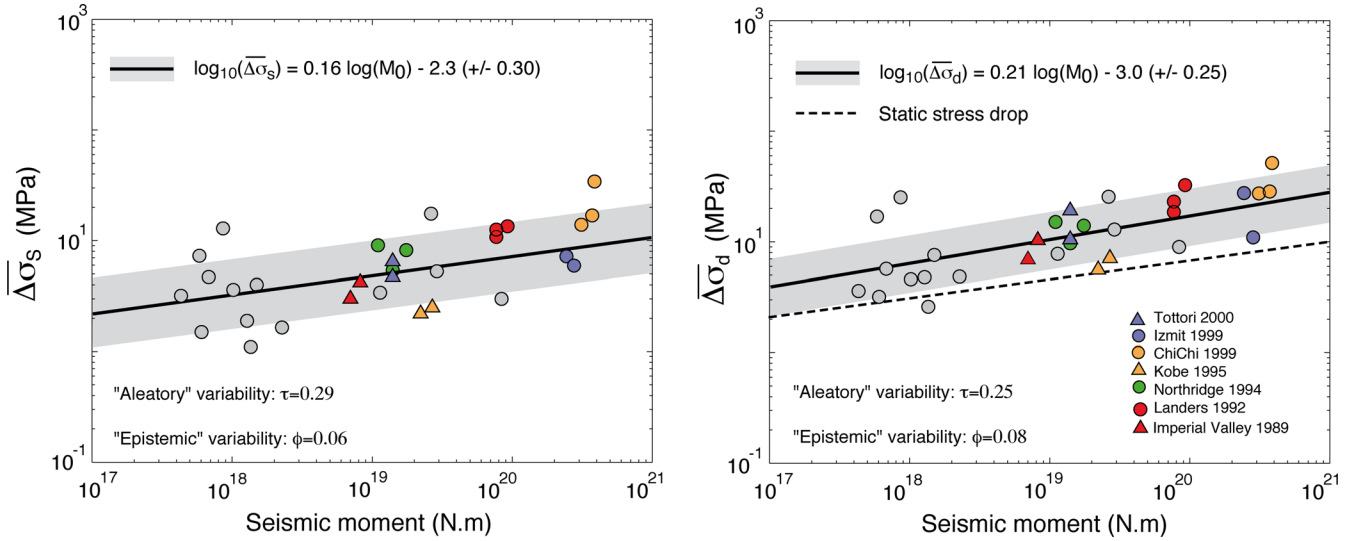

Figure 6. Scaling of static and dynamic stress drop with seismic moment; gray circles indicate events for which only a single model is available.

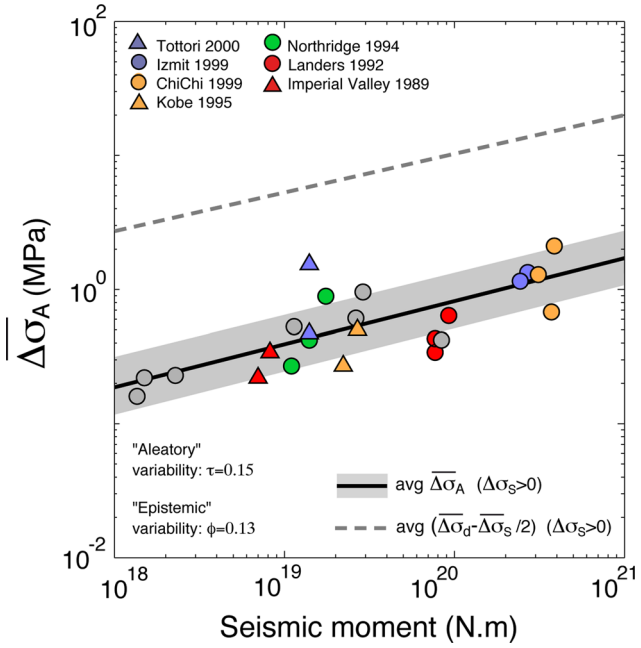

Figure 7. Scaling of apparent stress drop $\Delta\sigma_A$, averaged over the fault area with $\Delta\sigma_S > 0$. Events with negative values of $\Delta\sigma_A$ are not displayed and are not included in the regression. This corresponds to events with $M_w < 6$. For comparison, the scaling of $\Delta\sigma_S$ and ($\Delta\sigma_d - \Delta\sigma_S/2$, i.e. available elastic energy per unit of slip) are also represented. The gray circles indicate events for which a single model is available.

5 UNCERTAINTY ANALYSES AND VARIABILITY OF DYNAMIC SOURCE PARAMETERS

Although our analysis reveals a scaling of average dynamic properties with magnitude, the scatter is rather large, especially for the smaller events. Part of this scatter is epistemic, due to uncertainties in the input kinematic inversion models, while aleatory variability stems from the natural randomness of the rupture process. As an illustration of the epistemic uncertainty, Fig. 8 displays the static slip distributions for the 1994 Northridge earthquake obtained by different authors (Dreger 1994; Hartzell *et al*. 1996; Wald *et al*. 1996), as well as the inferred dynamic parameter distributions. Table 5 also reports the main features of the different inversion models. As for fracture energy and dynamic stress drop, this uncertainty is mainly due to variations in rise time values and the degree of roughness of the static slip distribution, both of which are inherently difficult to capture by kinematic source inversions (see Section 3).

To test if 'poorly resolved' kinematic models still provide robust information to examine the scaling of average dynamic source properties, we conduct an uncertainty analysis. The dispersion of the computed parameters around the average prediction is quantified by splitting the residuals into 'epistemic' and 'aleatory' components (see Fig. 5 for the case of fracture energy $\bar{G}$), thereby isolating the variability due to the uncertainties in the input finite-source rupture models from the event-to-event variability arising from the unpredictable randomness of the source process. We compute the 'epistemic' uncertainty, defined as (in the case of $\bar{G}$):

$$\phi = \frac{1}{N_m}\sqrt{\sum_{ij}\left(\log_{10}(\bar{G}_{calc.Ei,Mj}) - \log_{10}(\bar{G}_{pred.spec,Ei})\right)^2}, \qquad (7)$$

where N_m is the number of rupture models of events analysed ($N_m = 17$ in our study), $\bar{G}_{calc.Ei,Mj}$ is the value calculated for model M_j of event E_i, and $\bar{G}_{pred.spec.Ei}$ refers to the partial average prediction using only data from event E_i. The 'aleatory' variability is then defined as

$$\tau = \frac{1}{N_{evt}}\sqrt{\sum_{i}\left(\log_{10}(\bar{G}_{pred.spec.\ Ei}) - \log_{10}(\bar{G}_{pred.glob.\ Ei})\right)^2} \qquad (8)$$

where N_{evt} is the number of events, and $\bar{G}_{pred.glob.Ei}$ is the global average prediction for event E_i.

The resulting epistemic uncertainty remains small (less than a factor of 1.5, see Table 6), from which we conclude that the global scaling properties of the dynamic parameter revealed by our computations are robust.

The parameter that is least affected by uncertainties in kinematic inversion models is the static stress drop, for which $\phi \sim 0.06$, and an aleatory variability of $\tau \sim 0.3$. This remains small in comparison to many stress-drop estimates assuming a point source model. Cotton *et al*. (2013) have shown that such point-source analyses lead to a total variability $\sigma_{\log_{10}\Delta\sigma} \sim 0.6$, which may be attributed to uncertainties in the corner frequency measurement. Recently, Baltay *et al*. (2013) have proposed an alternative approach from the measurement of a_{rms} and obtain $\sigma_{\log_{10}\Delta\sigma} \sim 0.4$. Moreover, our uncertainty analysis for $\overline{\Delta\sigma_A}$ yields $\tau \sim 0.15$, which corresponds to a factor of ~1.5. This is also smaller than the errors reported for various methods based on integration of regional or teleseismic velocity records, giving factors larger than 2 and even as large as 10 (Pérez-Campos & Beroza 2001). Therefore, we claim that finite-source rupture models can provide robust alternative information to analyse the distribution of stress drop and apparent stress drop.

It is important to note that the epistemic uncertainty ϕ computed from eq. (7) only provides a quantitative measure of the variability due to uncertainties in the kinematic inversion models, that is in the input data. It does not include uncertainties due to the method proposed to calculate dynamic parameters. In addition, a rigorous analysis of the epistemic uncertainty would require a significantly larger data set, including multiple models for the whole set of earthquakes. Such a data set is not available presently.

6 DYNAMIC PARAMETERS VERSUS CUMULATIVE SLIP

Some recent studies adress the link between long-term properties of faults, like the degree of 'maturity', and earthquakes dynamics or ground-motion (e.g. Manighetti *et al*. 2007; Choy & Boatwright 2009; Radiguet *et al*. 2009). The fault maturity depends on the fault geometry and long-term fault history, that is age, maximum slip rate and cumulative displacement.

In this section, we show how static stress drop, fracture energy and apparent stress drop evolve with cumulative displacement for six of the 22 analysed earthquakes (Table 7). Estimates of cumulative displacement are from Radiguet *et al*. (2009), from the Fault Morphology Database (http://isterre.fr/recherche/equipes/mecanique-des-failles/observatoires-et-plateforme-de/article/fault-morphology-database) and from Yue *et al*. (2005) for the 1999 ChiChi earthquake. This analysis seems to indicate that static stress drop and fracture energy decrease with the amount of cumulative displacement (Fig. 9). Apparent stress drop also appears to decrease with cumulative displacement, aside from the 1999 Izmit earthquake for which the high apparent stress drop is consistent with the reported super-shear rupture velocity (e.g. Bouchon *et al*. 2002; Sekiguchi & Iwata 2002), thus implying that most of the available strain energy was radiated seismically. These tendencies,

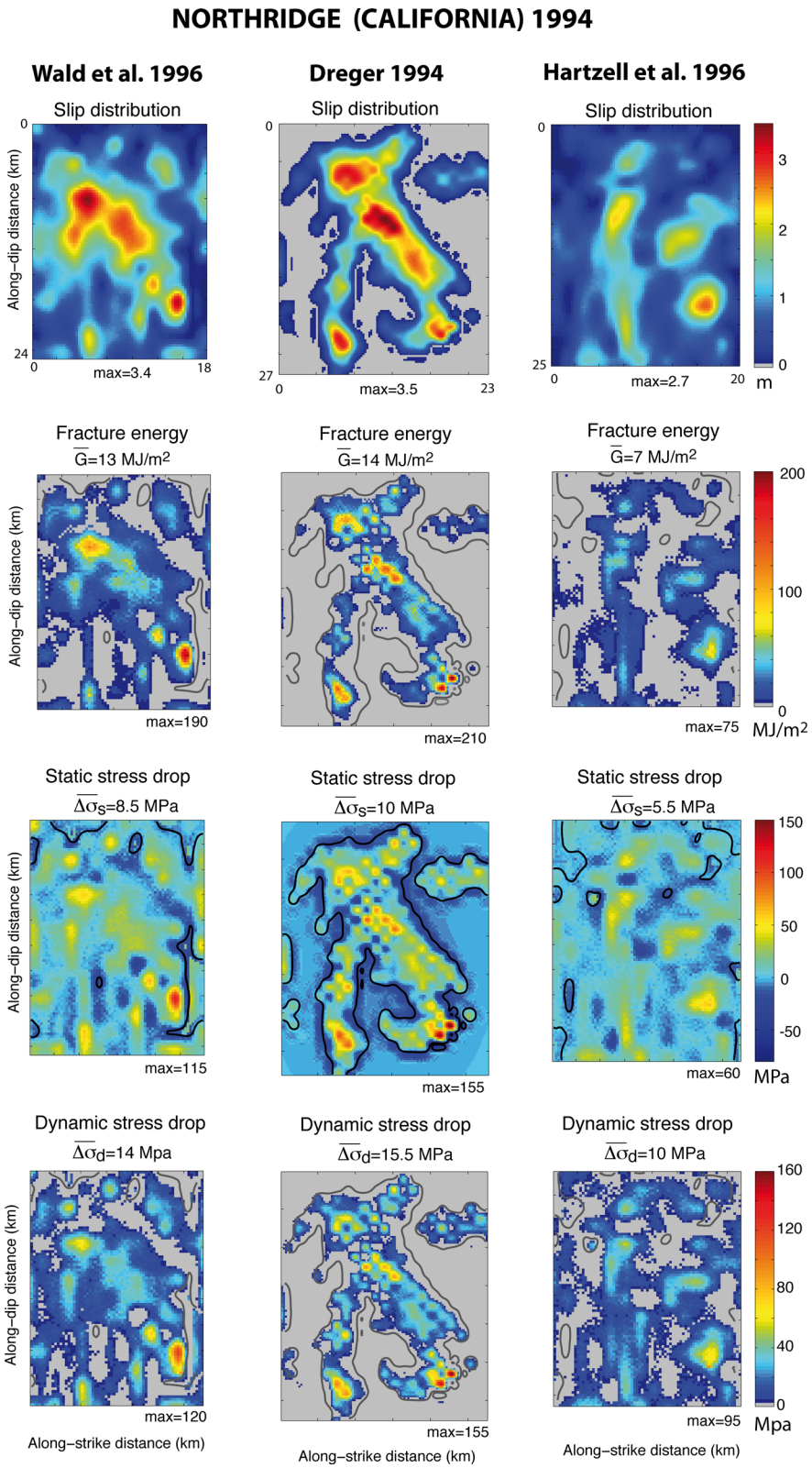

Figure 8. Static slip distributions and inferred dynamic parameter distributions obtained from different authors for the 1994 Northridge event. Contour-lines delineate the area on which dynamic parameters are averaged (static slip larger than 20 per cent of the mean slip). Distributions of apparent stress drop are not shown for simplicity. The average values $\Delta\sigma_A$ are 0.9, 0.3 and 0.4 MPa for Wald *et al*. (1996), Dreger (1994) and Hartzell *et al*. (1996), respectively.

Table 5. Inversion parameters used by different authors for the 1994 M 6.7 Northridge earthquake, and inferred values of averaged dynamic source quantities. Note that magnitudes are slightly different. Since G is expected to be magnitude-dependent (see next sections), we generated 'scaled' versions of the models of Hartzell *et al*. (1996) and Dreger (1994) to set all M_w to 6.80 (by simply scaling static slip).

Kinematic model	M_w	Slip function	Inverted data SGM	Inverted data Teleseismic	Inverted data GPS	Inverted rise time	G (MJ m^{-2})	G (scaled models)	$\Delta\sigma_s$ (MPa)	$\Delta\sigma_d$ (MPa)
Wald *et al*. (1996)	6.80	Three triangles (t_{tri} = 0.6 s, t_{shift} = 0.4 s)	38	13	26	1.4	13	13	8.5	14
Hartzell *et al*. (1996)	6.73	Three triangles (t_{tri} = 0.6 s, t_{shift} = 0.4 s)	35	–	–	1.4	7	10	5.5	10
Dreger (1994)	6.66	One triangle	–	8	–	1	14	25	10	15.5

Table 6. Values of 'aleatory' variability and 'epistemic' uncertainty of the inferred average dynamic source parameters.

Dynamic parameter	'Aleatory' variability ($\log_{10}$ units)	'Epistemic' uncertainty ($\log_{10}$ units)
Fracture energy	0.44	0.11
Dynamic stress drop	0.25	0.06
Static stress drop	0.30	0.06
Apparent stress drop	0.15	0.13

Table 7. Cumulative displacements of 6 of the 22 events analysed.

Event	M_w	Cumulative slip (km)
Parkfield	6.0	>150
Izmit	7.6	~85
ChiChi	7.6	~3
Landers	7.2	3.1–4.6
Imperial Valley	6.5	~24
Coyote Lake	5.9	~24

though supported by only a sparse dataset (six source models), may simply be explained by fault-plane surfaces tending to become smoother with increasing cumulative displacement (e.g. Brodsky *et al*. 2011; Candela *et al*. 2012b). Such smoother fault-surfaces are supposed to generate smoother slip distributions (Candela *et al*. 2011) associated with lower stress drop, smaller fracture energy and thus lower apparent stress drop (see Section 3.1 and Fig. 3).

7 DISCUSSION AND CONCLUSION

We conduct 3-D forward kinematic rupture simulations to infer the average fracture energy ($\bar{G}$), static stress drop ($\overline{\Delta\sigma_s}$), dynamic stress drops ($\overline{\Delta\sigma_d}$) and apparent stress drop ($\overline{\Delta\sigma_A}$) from 31 kinematic source inversion models of 21 crustal earthquakes with various styles of faulting. Our analysis reveals that: (1) $\bar{G}$ scales with seismic moment, corroborating previous results (e.g. Tinti *et al*. 2005a; Bizzarri 2010). We propose new scaling relations that are useful to constrain friction law parameters in spontaneous dynamic rupture simulations and physics based near-source ground-motion predictions; (2) $\overline{\Delta\sigma_s}$, $\overline{\Delta\sigma_d}$ and $\overline{\Delta\sigma_A}$ slightly increase with seismic moment, indicating that self-similarity (scale-independent stress-drop) would not be valid in the investigated magnitude range ($M_w \sim 6$–7.5) for non-point-source earthquake parameters; (3) $\Delta\sigma_S$ seems to decrease with cumulative slip, like $\bar{G}$ and $\overline{\Delta\sigma_A}$, but the tendency is less clear. Given the limited data set (six events) for this analysis this last conclusion remains tentative. (4) The epistemic uncertainty of $\bar{G}$, $\overline{\Delta\sigma_s}$, $\overline{\Delta\sigma_d}$ and $\overline{\Delta\sigma_A}$ (i.e. due to uncertainties in the input kinematic source inversion models) is approximately $\phi \sim 0.1$ (in $\log_{10}$ units), which corresponds to a factor ~1.3. This uncertainty remains small compared to many studies based on point-source models, reporting factors of ~4 for stress drop (Cotton *et al*. 2013) and larger than 2 for apparent stress drop (Pérez-Campos & Beroza 2001). Therefore, we claim that kinematic source inversion models provide robust alternative data to analyse the scaling of dynamic source properties. However, it is important to note that the bandwidth limitation in the input source models may lead to an underestimation of the dynamic parameters, especially for the apparent stress drop.

It is important to emphasize that the derived dynamic source parameters were inferred from stress changes calculated from forward kinematic rupture models, in which typically the stress on the fault drops continuously with slip, and stress gradually weakens at small and large slip (Figs 1 and 4). If we attempt to interpret these kinematic results in terms of friction models, one can imply that this pattern of stress change is 'dynamically inconsistent' because in a spontaneous rupture simulation these models would not necessarily propagate. However, it needs to be highlighted that the purpose of our calculations is not to derive friction models for dynamic rupture simulation, but average dynamic source parameters independent of the frictional properties.

7.1 Scaling of fracture energy

The physical phenomena involved in the observed scaling of $\bar{G}$ are not yet fully understood. $\bar{G}$ represents an observational mesoscopic parameter that contains all dissipative processes in the volume surrounding the crack tip. To understand its scaling, a holistic view of a fault is then required, in which a geometrically complex (fractal) fault is embedded in a 3-D medium that is heterogenous (fractured) at all scales. Campillo *et al*. (2001) and Latour *et al*. (2011) show that small-scale heterogeneities of fault strength may be represented by effective friction laws that reproduce the global behaviour of the fault rupture process. Such effective friction laws yield effective fracture energy that increases as the characteristic wavelength of the fault strength heterogeneity grows. This suggests that large faults, containing potentially larger scale strength heterogeneities, may have larger $\bar{G}$. The importance of fault heterogeneities for energy dissipation during the dynamic rupture is also pointed out by Ohnaka & Shen (1999) who observed larger slip weakening distances in case of larger scale fault-surface irregularities in lab friction experiments. Assuming that the roughness of slip distribution is controlled by the roughness of fault strength and fault topography (e.g. Candela *et al*. 2011), their results are consistent with our numerical simulations based on a k^{-2} kinematic source description, illustrating that $\bar{G}$ scales with the roughness degree of slip heterogeneities.

While the role of fault plane heterogeneity is fundamental in earthquake dynamics, off-fault damage constitutes another important factor of energy loss. Indeed, large crustal faults are associated with zones of damage rock characterized by high crack density (e.g. Ben-Zion & Sammis 2003). Andrews (2005) performed dynamic simulations in which the slip zone is modelled as a fault plane with off-fault dissipation according to a Coulomb yield condition. They found that energy loss, which can be mapped into G, is proportional

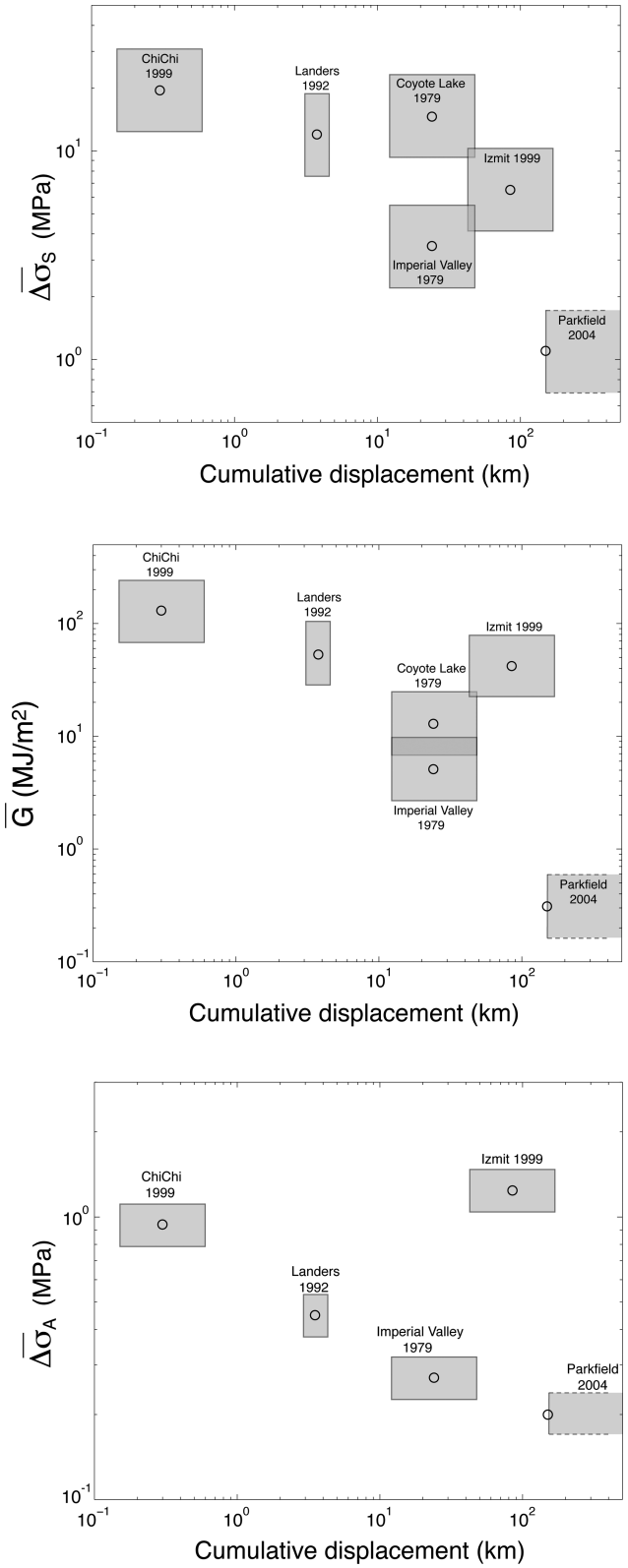

Figure 9. Static stress drop ($\Delta\sigma_S$), fracture energy (G) and apparent stress drop ($\Delta\sigma_S$) versus cumulative displacement, for six events for which data on cumulative fault offset are available. Boxes represents the approximate error bars—a factor of 1.3 for the dynamic parameters, based on the estimations of the with-event variability of Section 5 'Uncertainty analyses and variability of source parameters', and a factor of 2 assumed for the cumulative displacement.

to propagation distance, and hence tends to increase with earthquake size. Whereas the effect of heterogeneities in frictional properties potentially could be captured by kinematic source inversion (within the resolved frequency band), it is difficult to assess if kinematic models contain the effects of off-fault damage. Understanding the proportion of both processes mapped into G is an important question that could be addressed through dynamic simulations including off-fault plasticity (e.g. Templeton & Rice 2008; Dunham *et al*. 2011; Gabriel *et al*. 2013) or friction experiments including off-fault damage and various length scales of fault strength.

7.2 Scaling of stress drop and apparent stress drop

Our results suggest that $\overline{\Delta\sigma_s}$ and $\overline{\Delta\sigma_A}$ scale with magnitude, in contradiction to the classic self-similarity hypothesis of earthquake behaviour that implies scale-independent (constant) stress drop. Dalguer *et al*. (2008) points out that self-similarity may still hold for buried rupture events, but may be broken for surface rupture events only. Nevertheless, performing our analysis by screening out the surface rupture events does not change the scaling properties of the static stress drop, which still increases with seismic moment in the same manner.

Such a scaling of stress drop is also reported by Abercrombie & Rice (2005). The consistency between their and our findings is interesting as they use a completely independent approach and data. While we compute $\bar{G}$ and $\overline{\Delta\sigma_s}$ and then infer $\overline{\Delta\sigma_A}$ from energy-balance considerations, they obtain static and appparent stress drops from point-source estimates of corner frequency and radiated seismic energy. Next, they deduce fracture energy from the energy balance, and find that it scales with magnitude. The main advantage of their approach is that (1) the considered frequency band is not limited to ~1 Hz; (2) the analysed earthquakes are approximately from the same region (whereas we are constrained to mix different geologic-tectonic areas to create sufficient input data). The increase of $\overline{\Delta\sigma_s}$ inferred from both studies may still be controversial, because measures from corner frequency estimation are subject to large uncertainties (Cotton *et al*. 2013), while our estimates of $\overline{\Delta\sigma_s}$ reveal only a slight increase. Nevertheless, if both $\bar{G}$ and $\overline{\Delta\sigma_A}$ do increase with seismic moment, the available strain energy and $\Delta\sigma_S$ need to increase as well.

It is interesting to mention that many studies that reveal stress drop scaling (e.g. Mayeda & Malagnini 2009, 2010; Drouet *et al*. 2011) are based on analyses of aftershock sequences. On the contrary to main shocks, aftershocks occur in areas where stress has already been released. Our study, based on a data set of main shock analyses, presents an alternative viewpoint on scaling properties of stress drop.

7.3 Link between dynamic properties and cumulative slip

For six well-studied earthquakes, for which estimates of cumulative slip are available, we find that $\overline{\Delta\sigma_s}$ tends to decrease with cumulative slip. $\bar{G}$ and $\overline{\Delta\sigma_A}$ also appear to decrease with cumulative slip, though this trend is less clear. Note that these observations are based on a sparse data set, and therefore our conclusions are preliminary at this point. Nevertheless, the observed tendencies may be related to a simple physical process. Fault-plane surfaces tend to become smoother with cumulative displacement; smoother fault-surfaces may generate smoother slip distributions; smooth slip distributions are associated with lower stress drop, smaller fracture energy and lower apparent stress drop. For apparent stress drop,

this scaling behaviour may not apply if super-shear rupture occurs, which is favoured on particularly smooth faults. This was the case for the 1999 Izmit earthquake, associated with high $\overline{\Delta\sigma_A}$ and large cumulative slip. However, given the limited number of reported super-shear ruptures, there is no statistical meaningful database at present to further examine this scaling aspect in detail. Note that the rupture of the 1979 Imperial Valley was also reported to be locally super-shear, but the average rupture velocity was less than the shear wave velocity (Archuleta 1984).

As mentioned by Ben-Zion & Sammis (2003), the increasing amount of slip on faults may progressively destroy small-scale structures, and thereby produce more linear fault structures. However, Ben-Zion & Sammis (2003) claim that faults with large cumulative displacement are also associated with wider zones of damaged rock with a high crack density. Accordingly, there are two major competing effects that change G as a fault accumulates slip: on one hand faults become smoother, which tends to reduce G, while on the other hand, the zone of damaged rock widens, and tends to increase G. Unfortunately, our data set is too sparse to validate such mechanism.

Finally, it is important to note that cumulative slip represents a limited proxy of structural maturity of the fault, which is governed by other fault features like the age or the maximum slip rate (Manighetti *et al*. 2007). Structural maturity might be a better indicator of faults, and might be better correlated with earthquakes dynamic properties.

ACKNOWLEDGEMENTS

We thank Michel Bouchon, Fabrice Cotton, Francois Renard and Jean Virieux for discussions. This work as been supported by the NERA project (Network of European Research Infrastructures for Earthquake Risk Assessment and Mitigation) from the 7th Framework Programme by the European Commission. Partial support has been provided through grant ANR-2001-BS56–017 of the French 'Agence Nationale de la Recherche'. All the numerical computation have been performed on the IBM BlueGene/P *Shaheen* at the KAUST Supercomputing Laboratory.

REFERENCES

Abercrombie, R. & Rice, J.R., 2005. Can observations of earthquake scaling constrain slip weakening? *Geophys. J. Int.,* **162,** 406–424.

Allmann, B. & Shearer, P., 2009. Global variations of stress drop for moderate to large earthquakes, *J. geophys. Res.,* **114,** B01310, doi:10.1029/2008JB005821.

Andrews, D.J., 2005. Rupture dynamics with energy loss outside the slip zone, *J. geophys. Res.,* **110,** B01307, doi:10.1029/2004JB003191.

Archuleta, R.J., 1984. A faulting model for the 1979 Imperial Valley earthquake, *J. geophys. Res.,* **89,** 4559–4585.

Asano, K. & Iwata, T., 2006. Source process and near-source ground motions of the 2005 West Off Fukuoka Prefecture earthquake (2006), *Earth Planets Space,* **58,** 93–98.

Baltay, A., Hanks, T. & Beroza, G., 2013. Stable strss-drop measurements and their variability: implications for ground-motion predictions, *Bull. seism. Soc. Am.,* **103,** 211–222.

Ben-Zion, Y. & Sammis, C.G., 2003. Characterization of fault zones, *Pure appl. Geophys.,* **160,** 677–715.

Bizzarri, A., 2010. On the relations between fracture energy and physical observables in dynamic earthquake models, *J. geophys. Res.,* **115,** B10307, doi:10.1029/2009JB007027.

Bouchon, M., 1997. The state of stress on some faults of the San Andreas system as inferred from nearffield strong motion data, *J. geophys. Res.,* **102,** 11 731–11 744.

Bouchon, M., Toksoz, M.N., Karabulut, H., Bouin, M.P., Dietrich, M., Aktar, M. & Edie, M., 2002. Space and time evolution of rupture and faulting during the 1999 Izmit (Turkey) earthquake, *Bull. Seis. Soc. Am.,* **92**(1), 256–266.

Brodsky, E., Gilchrist, J., Sagy, A. & Collettini, C., 2011. Faults smooth gradually as a function of slip, *Earth planet. Sci. Lett.,* **302,** 185–193.

Brune, J.N., 1970. Tectonic stress and the spectra of shear waves from earthquakes, *J. geophys. Res.,* **75,** 4997–5009.

Burjanek, J. & Zahradnik, J., 2007. Dynamic stress field of a kinematic earthquake source model with *k*-squared slip distribution, *Geophys. J. Int.,* **171,** 1082–1097.

Campillo, M., Favreau, P., Ionescu, I.R. & Voisin, C., 2001. On the effective friction law of a heterogeneous fault, *J. geophys. Res.,* **106,** 16 307–16 322.

Candela, T., Renard, F., Schmittbuhl, J., Bouchon, M. & Brodsky, E., 2011. Fault slip distribution and fault roughness, *Geophys. J. Int.,* **187,** 959–968.

Candela, T., Renard, F., Bouchon, M., Schmittbuhl, J. & Brodsky, E., 2012a. Stress drop during earthquakes: effect of fault roughness scaling, *Bull. seism. Soc. Am.,* **101,** 2369–2387.

Candela, T., Renard, F., Klinger, Y., Mair, K., Schmittbuhl, J. & Brodsky, E., 2012b. Roughness of fault surfaces over nine decades of length scales, *J. geophys. Res.,* **117,** B08409, doi:10.1029/2011JB009041.

Causse, M., Chaljub, E., Cotton, F., Cornou, C. & Bard, P.Y., 2009. New approach for coupling k^{-2} and empirical Green's functions: application to the blind prediction of broadband ground-motion in the Grenoble basin, *Geophys. J. Int.,* **179,** 1627–1644.

Chi, W.C., Dreger, D. & Kaverina, A., 2001. Finite-source modeling of the 1999 Taiwan (Chi-Chi) earthquake derived from a dense strong-motion network, *Bull. seism. Soc. Am.,* **91,** 1144–1157.

Choy, G. & Boatwright, J., 2009. Differiential energy radiation from two earthquakes in Japan with identical M_w: the Kyushu 1996 and Tottori 2000 earthquakes, *Bull. seism. Soc. Am.,* **99,** 1815–1826.

Cocco, M. & Tinti, E., 2008. Scale dependence in the dynamics of earthquake propagation: evidence from seismological and geological observations, *Earth planet. Sci. Lett.,* **273,** 123–131.

Cocco, M., Spudich, P. & Tinti, E., 2006. On the mechanical work absorbed on faults during earthquake ruptures, in *Earthquakes: Radiated Energy and the Physics of Faulting*, Vol. 170, pp. 237–254, eds Abercrombie, R., McGarr, A., Kanamori, H. & Di Toro, G., Geophysical Monograph Series, American Geophysical Union.

Cotton, F. & Campillo, M., 1995. Inversion of strong ground motion in the frequency domain: application to the 1992 Landers, California, earthquake, *J. geophys. Res.,* **100,** 3961–3975.

Cotton, F., Archuleta, R. & Causse, M., 2013. What is sigma of stress drop? *Seismol. Res. Lett.,* **84,** 42–48.

Custodio, S., Liu, P.C. & Archuleta, R.J., 2005. The 2004 M_w 6.0 Parkfield, California, earthquake: inversion of near-source ground motion using multiple data sets, *Geophys. Res. Lett.,* **32,** L23312, doi:10.1029/2005GL024417.

Dalguer, L.A. & Day, S.M., 2007. Staggered-grid split-node method for spontaneous rupture simulation, *J. geophys. Res.,* **112,** B02302, doi:10.1029/2006JB004467.

Dalguer, L.A., Irikura, K., Zhang, W. & Riera, J.D., 2002. Distribution of dynamic and static stress changes during 2000 Tottori (Japan) earthquake: brief interpretation of the earthquake sequences; foreshocks, mainshock and aftershocks, *Geophys. Res. Lett.,* **29**(16), doi:10.1029/2001GL014333.

Dalguer, L.A., Miyake, H., Day, S.M. & Irikura, K., 2008. Surface rupturing and buried dynamic rupture models calibrated with statistical observations of past earthquakes, *Bull. seism. Soc. Am.,* **98,** 1147–1161.

Day, S.M., Yu, G. & Wald, D.J., 1998. Dynamic stress changes during earthquake rupture, *Bull. seism. Soc. Am.,* **88,** 512–522.

Delouis, B., Giardini, D., Lundgren, P. & Salichon, J., 2002. Joint inversion of InSAR, GPS, teleseismic & strong-motion data for the spatial and temporal distribution of earthquake slip: application to the 1999 Izmit mainshock, *Bull. seism. Soc. Am.,* **92,** 278–299.

Dreger, D.S., 1994. Empirical Greens-function study of the January 17, 1994 Northridge, California Earthquake, *Geophys. Res. Lett.,* **21,** 2633–2636.

Drouet, S., Bouin, M.P. & Cotton, F., 2011. New moment magnitude scale, evidence of stress drop magnitude scaling and stochastic ground-motion model for the French indies, *Geophys. J. Int.,* **187,** 1625–1644.

Dunham, E.M., Belanger, D., Cong, L. & Kozdon, J.E., 2011. Earthquake ruptures with strongly rate-weakening friction and off-fault plasticity, part 1: planar faults, *Bull. seism. Soc. Am.,* **101**(5), 2296–2307.

Fukuyama, E., Mikumo, T. & Olsen, K.B., 2003. Estimation of the critical slip-weakening distance: theoretical background, *Bull. seism. Soc. Am.,* **93,** 1835–1840.

Gabriel, A.A., Ampuero, J.P., Dalguer, L.A. & Mai, P.M., 2013. Source properties of dynamic rupture pulses with off-fault plasticity, *J. geophys. Res.,* **118,** 4117–4126.

Guatteri, M., Mai, P.M. & Beroza, G.C., 2004. A pseudo-dynamic approximation to dynamic rupture models for strong ground motion prediction, *Bull. seism. Soc. Am.,* **94,** 2051–2063.

Hartzell, S.H., 1989. Comparison of seismic waveform inversion results for the rupture history of a finite fault – application to the 1986 North Palm-Springs, California, earthquake, *J. geophys. Res.,* **94,** 7515–7534.

Hartzell, S.H. & Heaton, T., 1983. Inversion of strong ground motion and teleseismic waveform data for the fault rupture history of the 1979 Imperial Valley, California, earthquake, *Bull. seism. Soc. Am.,* **73,** 1555–1583.

Hartzell, S.H., Langer, C. & Mendoza, C., 1994. Rupture histories of eastern North American earthquakes, *Bull. seism. Soc. Am.,* **85,** 1703–1724.

Hartzell, S.H., Liu, P. & Mendoza, C., 1996. The 1994 Northridge, California, earthquake: investigation of rupture velocity, risetime & high-frequency radiation, *J. geophys. Res.,* **101,** 20 091–20 108.

Hernandez, B., Cotton, F. & Campillo, M., 1999. Contribution of radar interferometry to a two-step inversion of the kinematic process of the 1992 Landers earthquake, *J. geophys. Res.,* **104,** 13083–13099.

Hernandez, B., Cocco, M., Cotton, F., Stramondo, S., Scotti, O., Courboulex, F. & Campillo, M., 2004. Rupture history of the 1997 Umbria-Marche (central Italy) main shocks from the inversion of GPS, DInSAR and near field strong motion data, *Ann. Geophys.,* **47,** 1355–1376.

Horikawa, H., 2001. Earthquake doublet in Kagoshima, Japan: rupture of asperities in a stress shadow, *Bull. Seis. Soc. Am.,* **91,** 112–127.

Ide, S., 2002. Estimation of radiated energy of finite-source earthquake models, *Bull. seism. Soc. Am.,* **92,** 2994–3005.

Ide, S. & Takeo, M., 1997. Determination of constitutive relations of fault slip based on seismic waves analysis, *J. geophys. Res.,* **102,** 27 379–27 391.

Iwata, T. & Sekiguchi, H., 2002. Source process and near-source ground motion during the 2000 Tottori-ken Seibu earthquake, in *Proceedings of the 11th Japan Earthquake Engineering Symposium*, *Earthq. Eng. Res. Liaison Comm.,* Science Council of Japan, Tokyo.

Kanamori, H. & Brodsky, E., 2004. The physics of erthquakes, *Rep. Prog. Phys.,* **67,** 1429–1496.

Kanamori, H. & Riviera, L., 2004. Static and dynamic scaling relations for earthquakes and their implications for rupture speed and stress drop, *Bull. seism. Soc. Am.,* **94,** 314–319.

Kanamori, H. & Riviera, L., 2006. Energy partition during earthquake, in *Earthquakes: Radiated Energy and the Physics of Faulting,* Vol. 170, pp. 3–13, eds Abercrombie, R., McGarr, A., Kanamori, H. & Di Toro, G., Geophysical Monograph Series, American Geophysical Union.

Latour, S., Campillo, M., Voisin, C., Ionescu, I.R., Schmedes, J. & Lavallée, D., 2011. Effective friction law for small-scale heterogeneity in 3D dynamic rupture, *J. geophys. Res.,* **116,** doi:10.1029/2010JB008118.

Liu, H. & Helmberger, D.V., 1983. The near-source ground motion of the 6 August 1979 Coyote Lake, California, earthquake, *Bull. seism. Soc. Am.,* **73,** 210–218.

Ma, S. & Archuleta, R.J., 2006. Radiated seismic energy based on dynamic rupture models of faulting, *Bull. seism. Soc. Am.,* **111,** doi:10.1029/2005JB004055.

Ma, K.F., Song, T.R.A., Lee, S.J. & Wu, H.I., 2001. Spatial slip distribution of the september 20, 1999, Chi-Chi, Taiwan, earthquake (M_w 7.6) inverted from teleseismic data, *Geophys. Res. Lett.,* **27,** 3417–3420.

Mai, P.M., Somerville, P., Pitarka, A., Dalguer, L., Song, S., Beroza, G., Miyake, H. & Irikura, K., 2006. On scaling of fracture energy and stress drop in dynamic rupture models: consequences for near-source ground-motions, in *Earthquakes Radiated Energy and the Physics of Faulting,* Vol. 170, pp. 283–293, eds Abercrombie, R., McGarr, A., Kanamori, H. & Di Toro, G., Geophysical Monograph Series, American Geophysical Union.

Mai, P.M., Burjanek, J., Delouis, B., Festa, G., Francois-Holden, C., Monelli, D., Uchide, T. & Zahradnik, J. Source-inversion blindtest: initial results and further developments, 2007. *Eos Trans. AGU,* **88**(52), Fall Meet. Suppl., Abstract S53C-08.

Manighetti, I., Campillo, M., Bouley, S. & Cotton, F., 2007. Earthquake scaling, fault segmentation and structural maturity, *Earth planet. Sci. Lett.,* **253,** 429–438.

Mayeda, K. & Malagnini, L., 2009. Apparent stress and corner frequency variations in the 1999 Taiwan (Chi-Chi) sequence: evidence for a step-wise increase at $M_w < 5.5$, *Geophys. Res. Lett.,* **36,** L10308, doi:10.1029/2009GL037421.

Mayeda, K. & Malagnini, L., 2010. Source radiation invariant property of local and near-regional shear-wave coda: application to source scaling for the M_w 5.9 Wells, Nevada sequence, *Geophys. Res. Lett.,* **37,** L07306, doi:10.1029/2009GL042148.

Mena, B., Dalguer, L.A. & Mai, P.M., 2012. Pseudo-dynamic source characterization for strike-slip faulting, including stress heterogeneity and super-shear rupture, *Bull. seism. Soc. Am.,* **102**(4), 1654–1680.

Miyakoshi, K., Kagawa, T., Sekiguchi, H., Iwata, T. & Irikura, K., 2000. Source characterization of inland earthquakes in Japan using source inversion results, in *Proceedings of the 12th World Conf. Earthq. Eng.,* Auckland, New-Zeland.

Mikumo, T., Olsen, K.B., Fukuyama, E. & Yagi, Y., 2003. Stress-breakdown time and slip-weakening distance inferred from slip velocity functions on earthquake faults, *Bull. seism. Soc. Am.,* **93,** 264–282.

Noda, H., Lapusta, N. & Kanamori, H., 2013. Comparison of average stress drop measures for ruptures with heterogeneous stress change and implications for earthquake physics, *Geophys. J. Int.,* **193,** 1691–1712.

Ohnaka, M. & Shen, L., 1999. Scaling of the share rupture process from nucleation to dynamic propagation: implication of geometry irregularity of the rupturing surfaces, *J. geophys. Res.,* **104,** 817–844.

Pérez-Campos, X. & Beroza, G.C., 2001. An apparent mechanism dependence of radiated seismic energy, *Bull. seism. Soc. Am.,* **106,** 11 127–11 136.

Piatanesi, A., Tinti, E., Cocco, M. & Fukuyama, E., 2004. The dependence of traction evolution on the earthquake source time function adopted in kinematic rupture models, *Geophys. Res. Lett.,* **31,** L04609, doi:10.1029/2003GL019225.

Prieto, G.A., Thomson, D., Vernon, F., Shearer, P. & Parker, R., 2007. Confidence intervals for earthquake source parameters, *Geophys. J. Int.,* **168**(3), 1227–1234.

Radiguet, M., Cotton, F., Manighetti, I., Campillo, M. & Douglas, J., 2009. Dependency of near-field ground motions on the structural maturity of ruptured faults, *Bull. seism. Soc. Am.,* **99,** 2572–2581.

Rice, J.R., Sammis, C.G. & Parson, R., 2005. Off-fault secondary failure induced by a dynamic slip pulse, *Bull. seism. Soc. Am.,* **95,** 109–134.

Ripperger, J. & Mai, P.M., 2004. Fast computation of static stress changes on 2D faults from final slip distributions, *Geophys. Res. Lett.,* **31**(18), L18610, doi:10.1029/2004GL020594.

Schmedes, J., Archuleta, R.J. & Lavallée, D., 2010. Correlation of earthquake source parameters inferred from dynamic rupture simulations, *J. geophys. Res.,* **115,** B03304, doi:10.1029/2009JB006689.

Sekiguchi, H. & Iwata, T., 2002. Rupture process of the 1999 Kocaeli, Turkey, earthquake estimated from strong-motion waveforms, *Bull. seism. Soc. Am.,* **92,** 300–311.

Semmane, F., Campillo, M. & Cotton, F., 2005a. Fault location and source process of the Boumerdes, Algeria, earthquake inferred from geodetic and strong motion data, *Geophys. Res. Lett.,* **32,** L01305, doi:10.1029/2004GL021268.

Semmane, F., Cotton, F. & Campillo, M., 2005b. The 2000 Tottori earthquake: a shallow earthquake with no surface rupture and slip properties controlled by depth, *J. geophys. Res.,* **110,** B03306, doi:10.1029/2004JB003194.

Somerville, P. *et al.*, 1999. Characterizing crustal earthquake slip models for the prediction of strong ground motion, *Seismol. Res. Lett.,* **70,** 59–80.

Song, S.G. & Somerville, P., 2010. Physics-based earthquake source characterization and modeling with geostatistics, *Bull. seism. Soc. Am.,* **100**(2), 482–496.

Spudich, P. & Guatteri, M., 2004. The effect of bandwidth limitations on the inference of earthquake slip-weakening distance from seismograms, *Bull. seism. Soc. Am.,* **94,** 2028–2036.

Suzuki, W., Shin, A. & Sekiguchi, H., 2010. Rupture process of the 2008 Iwate-Miyagi Nairiku, Japan, earthquake derived from near-source strong-ground motion, *Bull. seism. Soc. Am.,* **100,** 256–266.

Templeton, E.L. & Rice, J.R., 2008. Off-fault plasticity and earthquake rupture dynamics: 1. Dry materials or neglect of uid pressure changes, *J. geophys. Res.,* **113,** B09306, doi:10.1029/2007JB005529.

Tinti, E., Spudich, P. & Cocco, M., 2005a. Earthquake fracture energy inferred from kinematic rupture models on extended faults, *J. geophys. Res.,* **110,** B12303, doi: 10.1029/2005JB003644.

Tinti, E., Fukuyama, E., Piatanesi, A. & Cocco, M., 2005b. A kinematic source time function compatible with earthquake dynamics, *Bull. seism. Soc. Am.,* **95,** 1211–1223.

Tinti, E., Cocco, M., Fukuyama, E. & Piatanesi, A., 2009. Dependence of slip weakening distance (*D*c) on final slip during dynamic rupture of earthquakes, *Geophys. J. Int.,* **177,** 1205–1220.

Wald, D.J., 1996. Slip history of the 1995 Kobe, Japan, earthquake determined from strong motion, teleseismic, and geodetic data, *J. Phys. Earth,* **44,** 489–503.

Wald, D.J. & Heaton, T.H., 1994. Spatial and temporal distribution of slip for the 1992 Landers, California, Earthquake, *Bull. seism. Soc. Am.,* **84,** 668–691.

Wald, D.J., Helmberger, D.V. & Heaton, T.H., 1991. Rupture model of the 1989 Loma-Prieta earthquake from the inversion of strong-motion and broad-band teleseismic data, *Bull. seism. Soc. Am.,* **81,** 1540–1572.

Wald, D.J., Heaton, T.H. & Hudnut, K.W., 1996. The slip history of the 1994 Northridge, California, earthquake determined from strong-motion, teleseismic, GPS & leveling data, *Bull. seism. Soc. Am.,* **86,** S49–S70.

Yoshida, S., Koketsu, K., Shibazaki, B., Sagiya, T., Kato, T. & Yoshida, Y., 1996. Joint inversion of near- and far-field waveforms and geodetic data for the rupture process of the 1995 Kobe earthquake, *J. Phys. Earth,* **44,** 437–454.

Yue, L.F., Suppe, J. & Hung, J.H., 2005. Structural geology of a classic thrust belt earthquake: the 1999 Chi-Chi earthquake, Taiwan (M_w 7.6), *J. Struct. Geol.,* **27,** 2058–2083.

Zhang, W., Iwata, T., Irikura, K., Pitarka, A. & Sekiguchi, H., 2004. Dynamic rupture process of the 1999 Chi-Chi, Taiwan, earthquake, *Geophys. Res. Lett.,* **31,** L10605, doi:10.1029/2004GL019827.